

Thermal Transport in Ampholytic Polymers: The Role of Hydrogen Bonding and Water Uptake

Patrick Hummel^{1,2}, Anna M. Lechner^{1,2}, Kai Herrmann^{1,2}, Philip Biehl^{3,4}, Carsten Rösse^{3,4}, Lisa Wiedenhöft^{3,4}, Felix H. Schacher^{3,4}, Markus Retsch^{1,2,}*

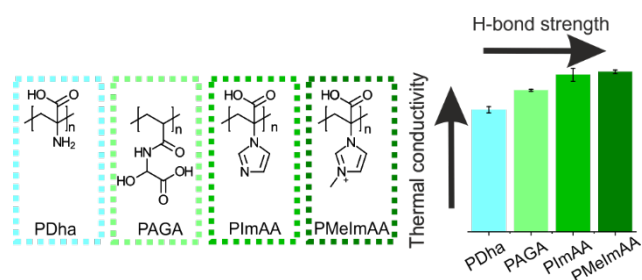
¹Department of Chemistry, Physical Chemistry I, University of Bayreuth, Universitätsstraße 30,
95447 Bayreuth, Germany

²Bavarian Polymer Institute, University of Bayreuth, Universitätsstraße 30, 95447 Bayreuth,
Germany

³Institute of Organic Chemistry and Macromolecular Chemistry, Friedrich Schiller University
Jena, Lessingstraße 8, D-07743 Jena, Germany

⁴Jena Center for Soft Matter (JCSM), Friedrich Schiller University Jena, Philosophenweg 7, D-
07743 Jena, Germany

*retsche@uni-bayreuth.de



KEYWORDS

Thermal conductivity; Fourier self-deconvolution; hydrophilic polymer; Photoacoustic method, effective medium model

ABSTRACT

The low thermal conductivity of amorphous polymers typically prevents their usage in thermal management applications. Therefore, increasing their intrinsic thermal conductivity poses an exciting scientific challenge. One approach is to promote attractive interchain interactions. Here, we investigate the thermal conductivity of several ampholytic polymers. This unique class of polymers offers H-bond donor and acceptor groups in each repeat unit and constitutes an one-component system. We use IR spectroscopy to characterize the bonding strength and motifs based on the carbonyl peak. For the dry ampholytic polymers, we find a correlation between H-bond strength and thermal conductivity. We also characterized the influence of hydration at various relative humidity conditions, which mostly led to an increase in thermal conductivity. This increase can be rationalized by the formation of a water-polymer nanocomposite material and can be described by volume-weighted mixing models.

Introduction

Easy processability, lightweight, low cost, and electrical insulation make polymers promising candidates for various applications in electronic devices. The continuously increasing energy density in such electronic devices demands a wholistic concept for thermal management at the same time.¹ The usually low thermal conductivity of polymers represents a significant obstacle in this context.

For that reason, the ambitious goal of polymer chemists is to create thermally highly conducting polymers. Similar to the discovery of (semi)conducting polymers, this would open up an entirely new space for the application of amorphous polymers. Two general strategies have been pursued to reach this goal: the creation of polymer (nano)composites and polymer processing. In the case of processing a variety of methods such as mechanical stretching²⁻³, electro-spinning⁴, and nano-templating⁵ have been investigated. In these cases, an increase in thermal conductivity is mostly attributed to a high chain orientation.⁶⁻⁷ The polymer chain orientation is often accompanied by some degree of crystallization. The chain alignment can be further enhanced by the proper design of the polymer backbone to promote stiffer polymer chains.⁸ Consequently, impressively high thermal conductivities, of around $20 \text{ W m}^{-1} \text{ K}^{-1}$, were measured along the axis of crystalline polymer fibers with a high modulus.² However, the radial thermal conductivity stays low.⁹ Even a commercial product is already available, making use of stretched polymers with a high degree of crystallinity. The organic heat spreader Temprion™ OHS (DuPont) with a crystallinity of 99.9 % demonstrates a remarkable in-plane thermal conductivity of $45 \text{ W m}^{-1} \text{ K}^{-1}$ and typical polymer-like cross-plane thermal conductivity of $0.2 \text{ W m}^{-1} \text{ K}^{-1}$. Amorphous polymers, in general, have a lower thermal conductivity than crystalline ones. However, their heat spreading capabilities would be less affected by the orientation in space owing to the random polymer coiling. Furthermore, the

processing of amorphous polymers is less sophisticated due to the lack of a nucleation and growth phase compared to (semi)crystalline samples. Ways to beat the intrinsically low thermal conductivity of amorphous polymers are mixing with highly conducting components or the introduction of functional groups.

In that regard, the field of (nano)composite materials has been actively investigated over the past years. The effective material properties strongly depend on a multitude of parameters such as the filler shape and composition, the interfacial interaction between filler and matrix, and the filler concentration.¹⁰⁻¹¹ Depending on the filler shape, anisotropic thermal transport properties may evolve at the same time.¹²⁻¹³

The introduction of functional groups to the polymer backbone or its side-groups is an alternative approach to increase the thermal conductivity. The main driving force for an increased thermal conductivity is stretching of the polymer to a more elongated conformation and an improved interchain transfer of the heat. Amorphous polymers with hydrogen bond-forming functional groups are consequently well suited to realize improved thermal conductivities.¹⁴ The strong hydrogen bonding between adjacent polymer chains could improve the transfer of thermal energy. In addition to this, the thermal conductivity can be further increased by the use of polyelectrolytes.¹⁵⁻¹⁶ Polyelectrolytes react sensitively to external stimuli such as ionic strength or pH, which influence the polymer conformation and polymer packing.

The engineering of these interchain interactions can lead to high thermal conductivities of up to $1.5 \text{ W m}^{-1} \text{ K}^{-1}$, as shown in amorphous polymer blends.¹⁷ However, demixing is a significant issue in polymer blends, and controversial findings on the role of H-bond were published.¹⁴ Miscibility is always an enormous challenge in polymer blends, and the resulting microstructure can be hard to characterize.

In this work, we present a new approach to prevent the issue of miscibility. Ampholytic polymers exhibit donor and acceptor groups for the formation of H-bonds covalently attached to one polymer chain, which inevitably prevents demixing. We present five different ampholytic polymers with a detailed characterization of their microstructure (measured by IR spectroscopy) and their thermal transport properties (measured by the photoacoustic method).

Materials and Methods

Polymer synthesis

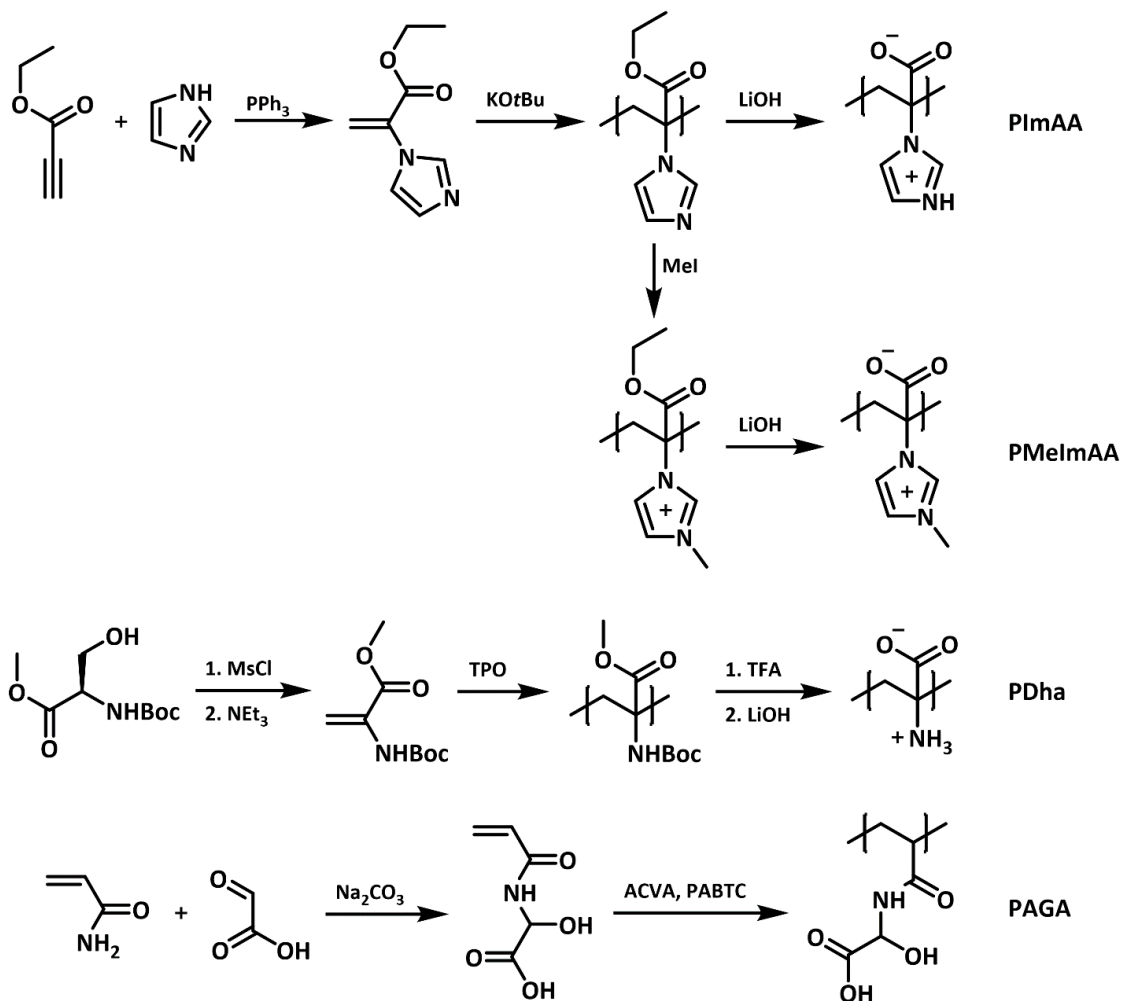
Synthesis of poly(2-(imidazole-1-yl)acrylic acid) (PImAA). The synthesis of ethyl 2-(imidazole-1-yl)acrylate (EImA) and anionic polymerization in tetrahydrofuran (THF) with potassium *tert*-butoxide (KO*t*Bu) as initiator, as well as the polymer modifications, were performed as described in the literature.¹⁸ The polymers were characterized by ¹H NMR (300 MHz, D₂O) and SEC (0.1 M NaCl/0.3 % TFA in water, P2VP calibration).

Synthesis of polydehydroalanine (PDha): PDha was synthesized as reported by Günther et al. or von der Lühe et al.¹⁹⁻²⁰ Briefly, a solution of 2.9 mg (0.0084 mmol) of Lucirin TPO in 300 μ L of 1,4-dioxane was added to 300 mg (1.49 mmol) of *tert*-butoxycarbonylaminomethyl acrylate (*t*BAMA; M:I = 200:1). The mixture was placed in an UV cube (100 W) for 5 min. Afterward, the polymer was precipitated in 4 mL *n*-hexane and subsequently deprotected. Therefore, 500 mg of the obtained *Pt*BAMA was dissolved in 7.5 mL of trifluoroacetic acid and stirred at 50 °C for one h. The mixture was precipitated in methanol. The so obtained PAMA was dissolved in 10 mL of 1,4-dioxane, and a saturated solution of LiOH (10 mL) was added. The mixture was stirred at 100 °C for three h and neutralized with diluted HCl_{aq}. During neutralization, PDha precipitated. PDha was characterized by ¹H NMR (300 MHz, D₂O/NaOD, pH 8).

Synthesis of poly(2-acrylamido glycolic acid) (PAGA): 2-Acryloylamido glycolic acid was synthesized as described in the literature.²¹ Reversible addition-fragmentation chain transfer (RAFT) polymerization was performed according to a previously published protocol²² with [M]:[CTA]:[I] = 145:1:0.3. PAGA was characterized by ¹H NMR (D₂O, 300 MHz) and SEC (0.1 M NaNO₃/ 0.05 % NaN₃, PEO calibration).

Synthesis of poly(methyl methacrylate) (PMMA): The RAFT synthesis of the PMMA was adapted from Mayadunne et al.²³ Therefore, 38.25 g (0.382 mol) MMA, 750.6 mg (2.17 mmol) 2-Cyano-2-propyl dodecyl trithiocarbonate (CPDTTC), 3.7 mg (0.0225 mmol) azobisisobutyronitrile (AIBN), and 11.9 g (0.129 mol) toluene were placed in a flask. The mixture was heated to 80 °C for 33.5 h. The polymer was precipitated in methanol.

Poly(acrylic acid) (PAA): was purchased from Sigma-Aldrich as a sodium salt solution. The pH of the solution was adjusted to 1. The sodium ions were removed by dialysis of the solution against Milli-Q water until constant pH.



Scheme 1. Synthesis of poly(2-(imidazole-1-yl)acrylic acid) (PImAA), poly(2-(3-methylimidazolium-1-yl)acrylic acid) (PMeImAA), poly(dehydroalanine) (PDha), and poly(2-acrylamido glycolic acid) (PAGA).

Table 1. Summary of the measured polymer properties. The density and c_p values were used for the determination of thermal conductivity.

Name	M_n [g mol ⁻¹]	PDI	Density [g cm ⁻³]	c_p [J g ⁻¹ K ⁻¹]
PImAA	5,500 ^{a)}	1.31 ^{a)}	1.48	1.045
PMeImAA	3,300 ^{a)}	1.45 ^{a)}	1.37	0.896
PDha	13,000 ^{b)}	2.5 ^{b)}	1.24	1.009
PAGA	28,500 ^{c)}	1.32 ^{c)}	1.22	1.245
PAA	15,000	-	1.26	1.202
PMMA	17,400 ^{d)}	1.15	1.15	1.217

^{a)} Determined by SEC using aqueous 0.3 % TFA/0.1M NaCl as eluent and calibrated against P2VP standards; ^{b)} Determined for the protected precursor of PDha by SEC using 0.1 % LiCl in DMAc as eluent and calibrated against PMMA standards; ^{c)} Determined by SEC using 0.1 M NaNO₃/ 0.05 % NaN₃ as eluent and calibrated against PEO standards, ^{d)} Determined by SEC using THF as eluent and calibrated against PMMA standards.

Sample preparation

Spin-coating

The polymers were dissolved in the respective solvent to achieve concentrations between 15 wt% and 25 wt%. PMMA was dissolved in toluene, PDha in DMSO, while all other polymers were processed from water. The solutions were then spin-casted on glass substrates with dimensions of 25x25 mm at 3000 rpm for 150 s. These samples were used for thermal conductivity measurements and IR investigations. The dry samples were kept in a vacuum oven at 100 °C for 24 h.

Humidity annealing

Saturated salt solutions in a desiccator achieved different relative humidities. We used MgCl₂, NaCl, and K₂SO₄ for relative humidities of 45 %, 77 %, and 92 %, respectively.²⁴ The spin-cast samples were equilibrated in the humid atmosphere for 24 h before further investigations. The

transducer layer surface is shown in Figure S10 and demonstrates holes or cracks. Therefore, equilibration with the environment is not prevented by the evaporated transducer layer on top of the polymer. PA, AFM, and IR measurements were conducted immediately after receiving the samples from the humidity adjusted desiccator.

Thermal conductivity measurements

The photoacoustic (PA) method was used to determine the thermal conductivity of the spin-coated polymer films.²⁵⁻²⁶ A gold transducer layer was applied to the top of the sample before the measurement. The sample is fixed to the measurement cell. The cell is gas-tight and filled with 20 psi helium. A modulated laser heats the transducer layer periodically. The induced temperature change on the surface of the sample leads to an acoustic wave propagating into the gas. The acoustic signal is detected by a microphone and coupled to a lock-in amplifier. The frequency-dependent phase shift between the modulated laser beam and the acoustic wave is measured. The experimental data are fitted by a multilayer model, describing the temperature distribution in the sample. The primary fitting result is the total layer resistance. Dividing the total layer resistance by the film thickness, the effective thermal conductivity is obtained. Each sample was measured three times. The mean values of these measurements are presented with the standard deviations as error bars. The humidity dependent data were measured without additional external control of the surrounding humidity. We did not observe a drift in the photoacoustic signal during the measurement time and conclude that the humidity water uptake remains constant for this duration (Figure S1c). More details can be found in the Supporting information section S1.

Fourier-transform infrared spectroscopy

The Fourier-transform infrared (FTIR) measurements were conducted on a Bruker (Billerica, MA, USA) Vertex 70 IR spectrometer with an attenuated total reflection (ATR) measurement unit.

The measurements were performed from 380 cm^{-1} to 4000 cm^{-1} with a resolution of 4 cm^{-1} and 128 scans. The samples were taken from the desiccators or vacuum oven, respectively, and directly measured under ambient conditions. Normalized spectra were used to calculate the difference spectra relative to the dry polymer samples.²⁷ Therefore, the normalized spectrum of the dry sample was subtracted from the spectra at the different relative humidities. The CH_2 deformation vibration at 1450 cm^{-1} was used as a reference peak for normalization, which is unaffected by water adsorption.

Fourier self-deconvolution

Fourier self-deconvolution (FSD) is a mathematical method to increase spectral resolution. By this, it is possible to separate overlapping absorption bands in an IR spectrum.²⁸ We applied the FSD according to Hu et al.²⁹ The software OPUS 7.5 (Bruker, Billerica, MA, USA) was used for all steps. First, the carbonyl region (between 1800 cm^{-1} and 1540 cm^{-1}) was cut-off. A baseline correction with one iteration was performed, and the spectrum was smoothed by 5-9 points. In the next step, the FSD was performed with a Lorentzian shape with a half-bandwidth of 25, and a noise reduction of 0.30. Another baseline correction was conducted before the peaks were selected according to the minima of the second derivative of the initial spectrum. Finally, the peaks were fitted with a Gaussian profile with the Levenberg-Marquardt method.

Differential scanning calorimetry

Differential scanning calorimetry (DSC) measurements were performed on a TA instruments Discovery DSC 2500. Two heating cycles were conducted; only the second cycle was used for evaluation. The temperature profile ranged from -40 °C to 140 °C using a heating rate of 10 K min^{-1} with a nitrogen flow of 50 mL min^{-1} . The measurements are shown in Figure S8.

Modulated DSC (MDSC) measurements were performed to determine the c_p of the samples. The optimum MDSC parameters have been calculated and evaluated following the instructions described in the literature.³⁰ The modulations in the transition-range and the modulation period were controlled and adjusted to a heating rate of 2 K min^{-1} , a period of 80 sec, and an amplitude of 1.6 K. The final samples were measured in hermetic pans to avoid loss of water during the measurement. The experiments were performed in a temperature range from 5 to 60 °C. The c_p at 25 °C of each polymer is given in Table 1 **Scheme 1**. Synthesis of poly(2-(imidazole-1-yl)acrylic acid) (PIAA), poly(2-(3-methylimidazolium-1-yl)acrylic acid) (PMeImAA), poly(dehydroalanine) (PDha), and poly(2-acrylamido glycolic acid) (PAGA).

Table 1.*Helium pycnometer*

An Ultrapyc 1200e (Quantachrome Instruments, Boynton Beach, FL, USA) was used for the determination of the density of the dry samples. Before each run, the volume of the measurement cell was calibrated. Subsequently, a defined mass of the polymer was put into the cell. The volume of the polymer was determined by 100 runs. The division of mass and volume calculated the density. The obtained values are summarized in Table 1.

Results and Discussion

We investigate the effective thermal conductivity of four different ampholytic polymers, poly(dehydroalanine) (PDha), poly(2-acrylamido glycolic acid) (PAGA), poly(2-(imidazole-1-yl)acrylic acid) (PIImAA), and its methylated derivative poly(2-(3-methylimidazolium-1-yl)acrylic acid) (PMeImAA, Figure 1a). All polymers have at least two different functional groups per repetition unit. We also analyzed poly(acrylic acid) (PAA) with only one functional group, which was reported to play a crucial role in the formation of a highly conducting pathway.¹⁷ Poly(methyl methacrylate) is not able to form hydrogen bonds and was also measured as a reference system.

We start our analysis by the polymer characterization under dry conditions, i.e., after storing the samples in a vacuum oven. In the IR spectra in Figure 1b, it can be seen that, except PMMA, all polymers form intra- and intermolecular hydrogen bond interactions as indicated by the broad bands between 2500 cm⁻¹ and 3600 cm⁻¹. These bands originate from the O-H and N-H stretching vibrations. OH-wagging at 900 cm⁻¹ is another indicator for the presence of COOH under these vacuum dried conditions. This band is broad due to various spatial orientations of the H-bond

forming functional groups. Due to this variety of possible bonds, the underlying C-H stretching vibrations, and several overtones, this region of an IR spectrum is challenging to evaluate.

We, consequently, focus our analysis on another strong peak connected to hydrogen bonds: the carbonyl stretching vibration around 1700 cm^{-1} . This peak is very strong, possesses a small FWHM, and is sensitive to the local environment.^{29,31-32} Therefore, it provides a suitable target for further investigations of H-bonds. Furthermore, it was shown that the absorption coefficient of the carbonyl stretching vibration, in comparison to the O-H and N-H stretching, does not depend significantly on the strength of the H-bonds.³³⁻³⁴ One disadvantage is that H-bonds between functional groups without a carbonyl group contribution cannot be resolved. A first indication of the strength of a hydrogen bond is the position of the carbonyl peak, whereby lower frequencies indicate an increasing strength of the H-bond.³⁵ We see a systematic shift of the carbonyl peak from PAA to PMeImAA, indicating an overall increase in strength of the carboxylic H-bonds.

The effective thermal conductivities (Figure 1c) show typical values for water-soluble amorphous polymers compared to values reported in the literature (shaded area).¹⁴ Comparing our values for PMMA ($0.16\text{ W m}^{-1}\text{ K}^{-1}$) and PAA ($0.31\text{ W m}^{-1}\text{ K}^{-1}$) with the literature ($0.20\text{ W m}^{-1}\text{ K}^{-1}$ ¹¹⁴ and $0.34\text{ W m}^{-1}\text{ K}^{-1}$ / $0.37\text{ W m}^{-1}\text{ K}^{-1}$ ¹¹⁴) we find slightly lower values. The lower values are reasonable since the PA method determines the total layer resistance of the sample. The effective thermal conductivity is calculated based on the polymer film thickness. Also, it takes the thermal resistances between the polymer layer and the support structure and transducer layer, respectively, into account. We attribute the relatively large standard deviation of the PImAA sample to the lowest layer thickness ($< 1\ \mu\text{m}$) of the PImAA sample, which reduces the fitting accuracy.

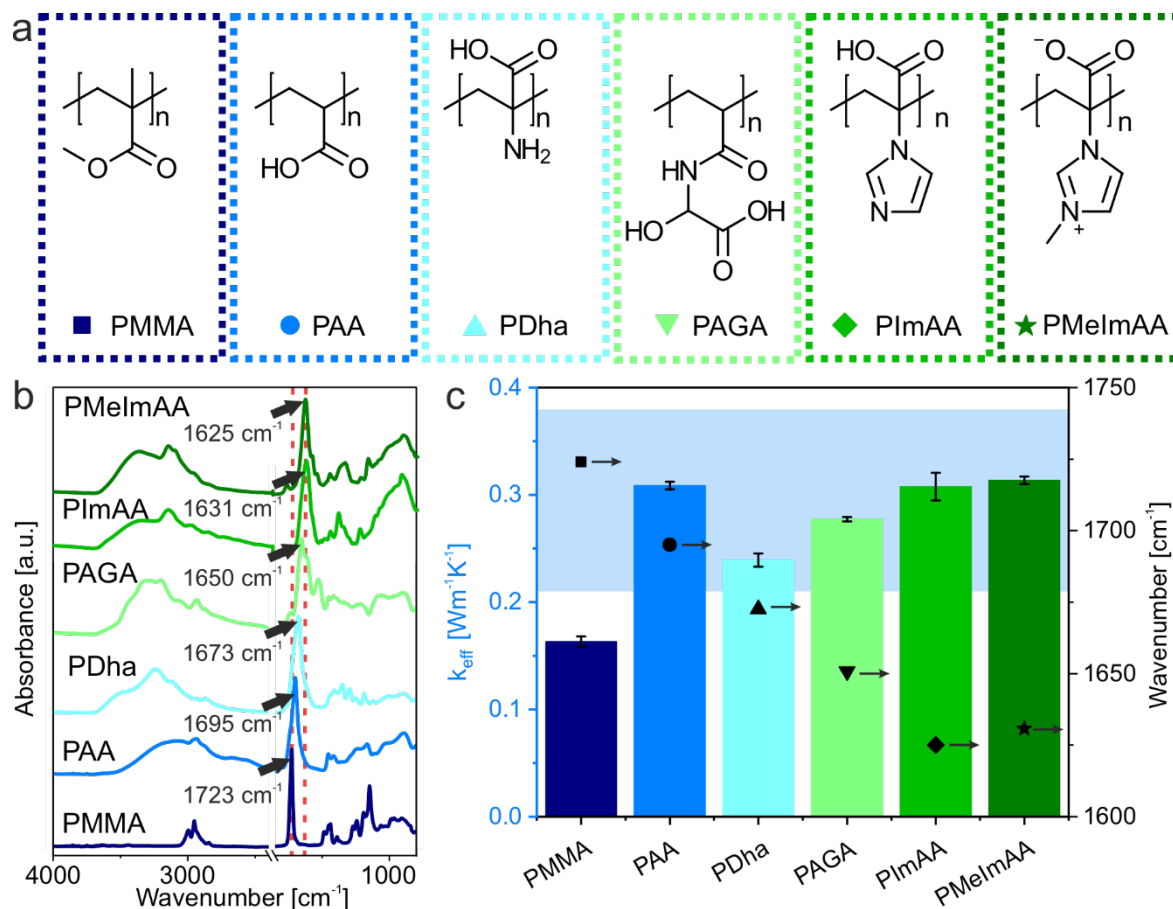


Figure 1. a) Structure of the ampholytic polymers and the reference polymers PAA and PMMA. The ampholytic polymers have at least two functional groups per repetition unit. b) IR spectra of all investigated polymer samples in the dry state. The red dashed lines present the carbonyl peak position of PMMA and PMeImAA, respectively. c) The measured effective thermal conductivity of all samples (solid bars). The thermal conductivity correlates with the peak position (black symbols) of the carbonyl band measured by IR spectroscopy (except for PAA). The light blue area indicates the range of literature values for amorphous, water-soluble polymers.¹⁴

Considering the systematic increase in H-bond strength derived from the carbonyl peak position, we find the expected increase in thermal conductivity for the ampholytic samples under

investigation. Rather unexpected from this point of view is the exceptionally high thermal conductivity of PAA.

For further insight into the strength of the H-bonds, we provide a detailed analysis of the IR spectra. We base our analysis on a Fourier self-deconvolution (FSD) of the carbonyl resonance between 1600 and 1750 cm^{-1} , according to Hu et al.²⁹ The fitted spectra are shown in Figure 2. The peaks are assigned to different configurations of the carbonyl group. Dark yellow is anhydrides (1805 cm^{-1} to 1760 cm^{-1}), green is free carbonyl groups (1740 cm^{-1} to 1730 cm^{-1}), cyan is the terminal oligomeric form of carboxylic acid (1716 cm^{-1} to 1680 cm^{-1}), blue is the cyclic dimer (1700 cm^{-1} to 1665 cm^{-1}), and grey-blue is the inner oligomeric form (1675 cm^{-1} to 1650 cm^{-1}). These peaks can be found in all samples containing a carboxylic acid group. The assignment is based on Dong et al.³¹, who investigated different H-bond motifs in PAA samples. The introduction of amino-groups in our ampholytic polymers introduces additional peaks marked in purple, ascribed to H-bonds with primary or secondary amino groups (PDha and PAGA). A final category of H-bonds is assigned to the interaction of the carbonyl group with the imidazole ring in PImAA and PMeImAA depicted in dark blue. Further contributions arising from vibrations other than the carbonyl stretching, like NH bending vibration/Amide II and vibrations of the aromatic ring, are summarized in orange. As a consequence, the orange bands were excluded for the evaluation of the carbonyl ratio.

The relative contribution of all these different classes of hydrogen bonds is summarized in Figure 2b. Most notably, PAA comprises a range of strongly coordinated H-bonds (dimer, inner, terminal) and even covalently condensed moieties (anhydride). The interplay of these structural motifs facilitates thermal transport between the polymer chains. Please note that the strength of the H-bond is lowest in the case of PAA compared to all other ampholytic polymers (Figure 1b, 1723

cm⁻¹ peak position of the carbonyl band). Thus the bonding scheme in PAA may additionally facilitate an elongated conformation, which also improves thermal transport. As soon as an additional functional group is introduced (NH₂ in the case of PDha), the thermal conductivity drops considerably. However, the nature of the H-bond environment is still comparable to PAA. Merely the anhydride and free-carboxyl bonds are replaced by O-H-N moieties (“other bonds” in Figure 2b). The overall stiffer carbonyl peak (1695 cm⁻¹) should even favor a higher thermal conductivity. Thus it is difficult to unambiguously relate the thermal conductivity reduction to subtle differences in the way hydrogen bonds are formed in the respective polymers. Additional contributions, such as the side chain structure¹⁵ or the influence of the side groups on the polymer morphology⁸, are important at the same time. Thus, the alleged beneficial influence of additional hydrogen bonds to the primary amino-group is counteracted by conformational changes that cannot be resolved by IR characterization. The transition from PDha to PAGA, PImAA, and PMeImAA demonstrates a monotonic increase in the class of other hydrogen bonds. Along this direction, the strength of the carbonyl bond also increases. The combination of both effects translates into the general trend of increasing thermal conductivity.

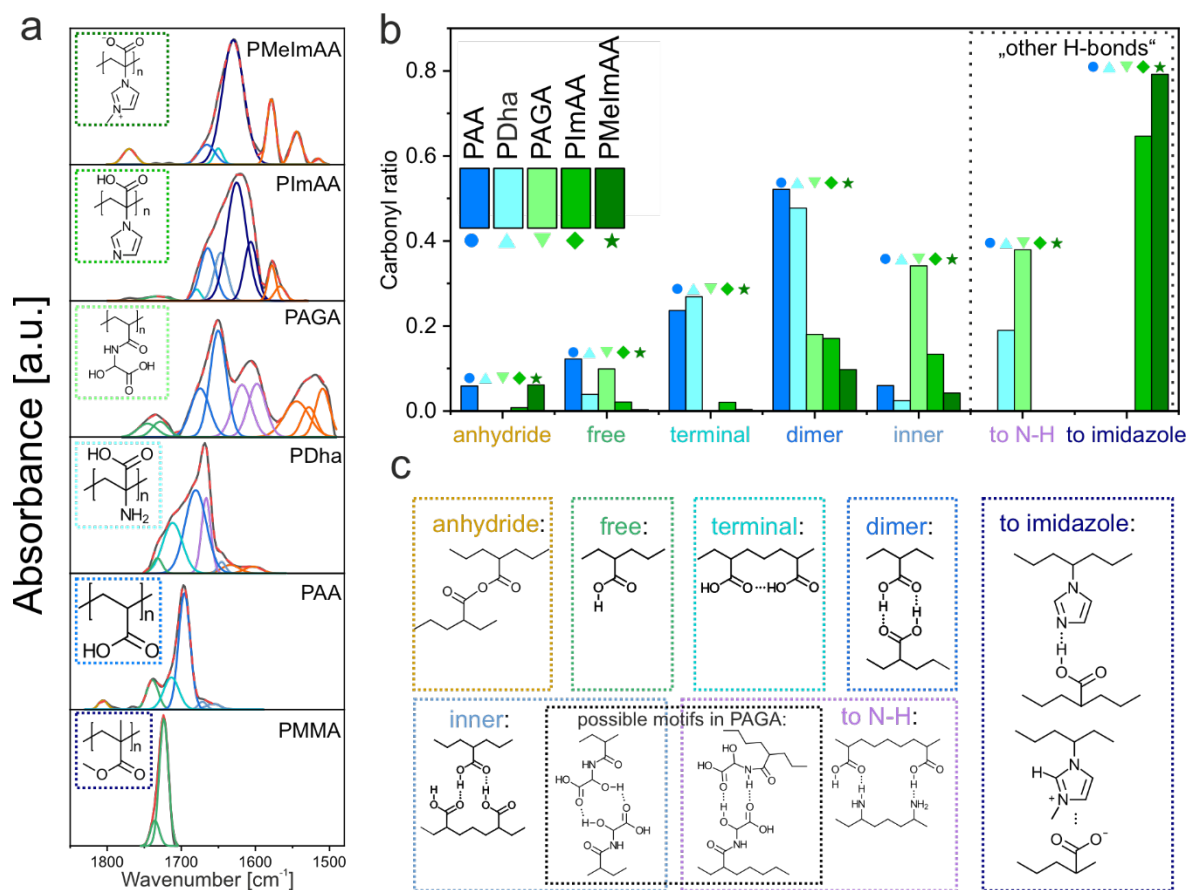


Figure 2. a) Deconvoluted IR spectra of all investigated samples. The films were dried before the measurements. b) The relative ratio of different motifs of the carbonyl bond. c) Schematic illustration of different H-bond motifs.

PAA and all herein used ampholytic polymers are strongly sensitive to humidity. We, consequently, determined its influence on the effective thermal conductivity. We gravimetrically measured the moisture content after prolonged exposure to specific humidities (Figure 3a). PMMA, as a control, demonstrates no sensitivity to increasing humidity. PAA exhibits a considerable absorption of water on the order of 40 %, whereas, in the case of the herein used, ampholytic polymers values from 35 % to 60 % are found. The quaternized PMeImAA exhibits the most significant water uptake and doubles its weight. These mass changes are comparable to

literature data on PAA³⁶ and other polyelectrolytes³⁷, respectively. The uptake of water influences not only the H-bonding within the polymers, but also the specific heat capacity and density. Both quantities are highly relevant when determining the thermal conductivity under these conditions. The measurement of the effective polymer density at various humidity conditions is not possible in a direct manner. We, therefore, used the measured moisture content to calculate the humidity dependent density. The specific heat capacity was determined experimentally by MDSC measurements, using hermetic pans (Figure 3b). The shaded areas indicate the expected c_p based on a mass-weighted mixing model considering the measured moisture contents. Whereas the overall trend of an increasing c_p is well captured in all cases, some degree of variability in a range of $\sim 20\%$ is seen. This variation can be explained by the difficulty of accurately retaining the moisture uptake and polymer conformation during the measurement itself.

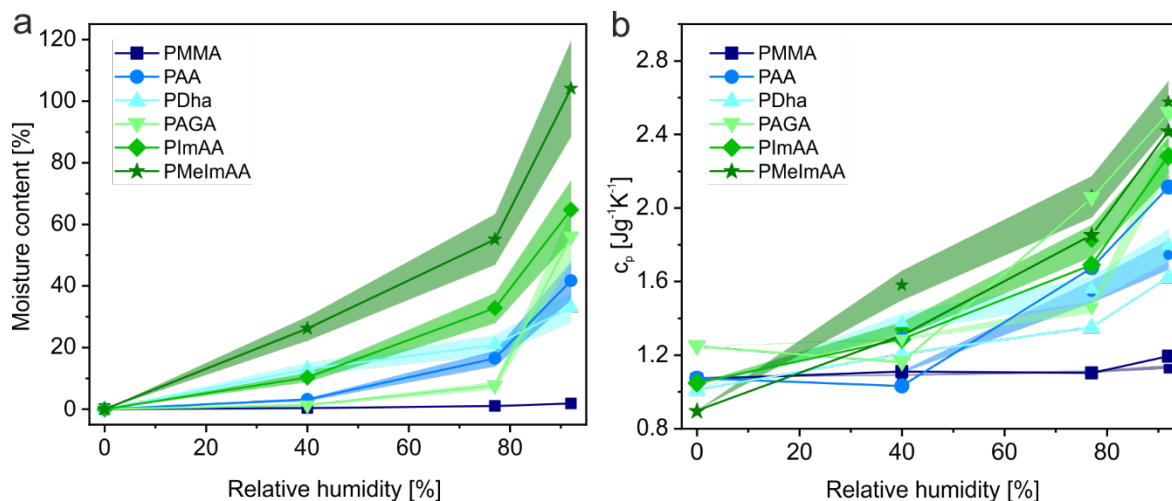


Figure 3. Humidity dependence of the samples. a) Moisture content increases with humidity for all polymers with functional groups. Shaded areas mark the variability. b) c_p , measured by MDSC, increases with humidity (solid lines and symbols). Shaded areas rationalize the expected trend of the c_p based on the water uptake in a) calculated by a mass-weighted mixing model.

The uptake of water also affects the polymer microstructure and H-bond environment. Consistently with our previous analysis, we used FSD of the carbonyl peak of our FTIR spectra. Figure 4 summarizes three distinct cases: PAA, PImAA, and PMeImAA. The spectra show a distinctly different way of water uptake in the case of PAA compared to PImAA and PMeImAA. In the literature, there is a differentiation between unbound and bound water.^{36,38} We define bound water as directly coordinated to the polymer, while unbound water interacts with other water molecules and forms clusters.

Our results of the absorbed amount of water in PAA (moisture content of 0.42 g/g polymer) are in good agreement with the literature value (0.47 g/g polymer).³⁶ Also, the FTIR difference spectrum is in good agreement with the findings of Daniliuc et al.³⁶ They reported a negative contribution in the difference spectra for free C=O (around 1735 cm⁻¹) and dimer (around 1700 cm⁻¹) and a positive peak between 1672 and 1634 cm⁻¹. The negative contributions are attributed to disconnected polymer-polymer interactions, while the positive contributions are newly formed polymer-water interactions.³⁶ They interpreted the spectra such that only bound water exists in their PAA sample.

Despite a higher moisture content, the difference spectra of PImAA and PMeImAA show overall fewer variations. Although the negative contributions between 1675 cm⁻¹ and 1600 cm⁻¹ represent disconnected polymer-polymer interactions, the overall lack of significant positive contributions indicates that the water is adsorbed in a less bound state in the case of PImAA and PMeImAA. The variation between these two polymers is smaller since polymers with similar functional groups show similar peaks in IR spectroscopy when ad/absorbing water.³⁹ The same data evaluation and representation for PDha and PAGA are summarized in Figure S8.

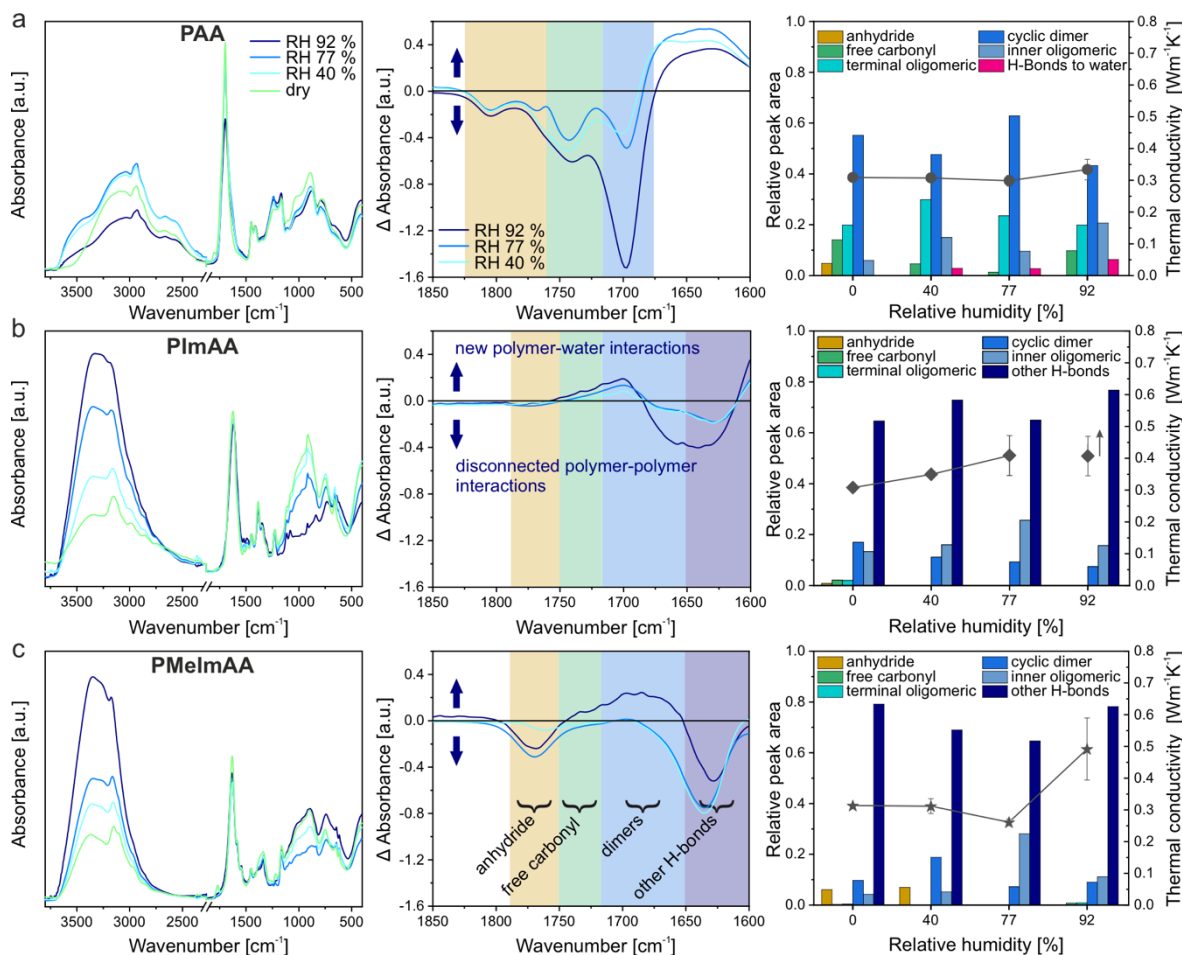


Figure 4. From left to right: IR-spectra of samples stored at different relative humidity. Difference spectra in the region of the carbonyl stretching vibration. The relative peak area of different H-bond structures dependent on the relative humidity. (a) PAA, (b) PImAA and (c) PMeImAA.

When considering the deconvoluted peaks (right panels of Figure 4), one has to be cautious while interpreting the respective contributions. The major difficulty is that the thermal conductivity is governed by various parameters, which was already pointed out in the discussion of the dry samples. We can, however, extract reasonable trends. PAA shows that the adsorption of bound water hardly influences the thermal conductivity. Consequently, bound water intercalates tightly between the PAA chains without affecting its conformation nor impeding interchain thermal

transport. The IR spectra of PImAA do not show significant changes in the carbonyl peak region. Consequently, the uptake of bound and unbound water itself seems to be the driving force for the monotonic increase in thermal conductivity. PMeImAA hints towards the fact that the creation of inner oligomeric groups on the expense of anhydride, cyclic dimer, and charged heterocycle interactions impedes thermal transport up to the humidity of $RH \sim 77\%$. Lastly, considering reports in the literature, the uptake of water was also reported to increase the effective thermal conductivity strongly. Mehra et al.⁴⁰ worked with polyvinylalcohol (PVA) and ascribed the thermal conductivity increase to the formation of thermal bridges by bound water molecules. All these examples demonstrate that the influence of humidity on the thermal transport in hydrophilic polymers is hard to predict and certainly depends on the specific polymer/water combination.

Whereas the previous discussion focused on a microscopic interpretation of inter- and intramolecular interaction between the constituting polymers, we also want to draw the attention to an alternative consideration comprising a much more coarse-grained point of view. The uptake of unbound water can be understood as a way to generate a two-phase material, where water clusters are formed.³⁸ This heterogeneous material can then be analyzed in a similar way to other nanocomposite materials using effective medium models as described by Carson⁴¹. For this, we use the vacuum (dry) polymer thermal conductivity as the pure phase of one component and literature data of the thermal conductivity of water as the second component. In combination with our data of the moisture uptake (Figure 3a) and two volume-weighted mixing models (parallel mixing model and effective medium model⁴¹), the humidity-dependent thermal conductivity is calculated (Figure 5). For PDha, PAGA, and PImAA, both mixing models describe the experimental data adequately well, particularly when considering the accuracy of the mixing models themselves and the thermal conductivity determination. For the case of PAA, where a high

amount of bound water can be expected, both mixing models systematically overestimate the effective thermal conductivity.

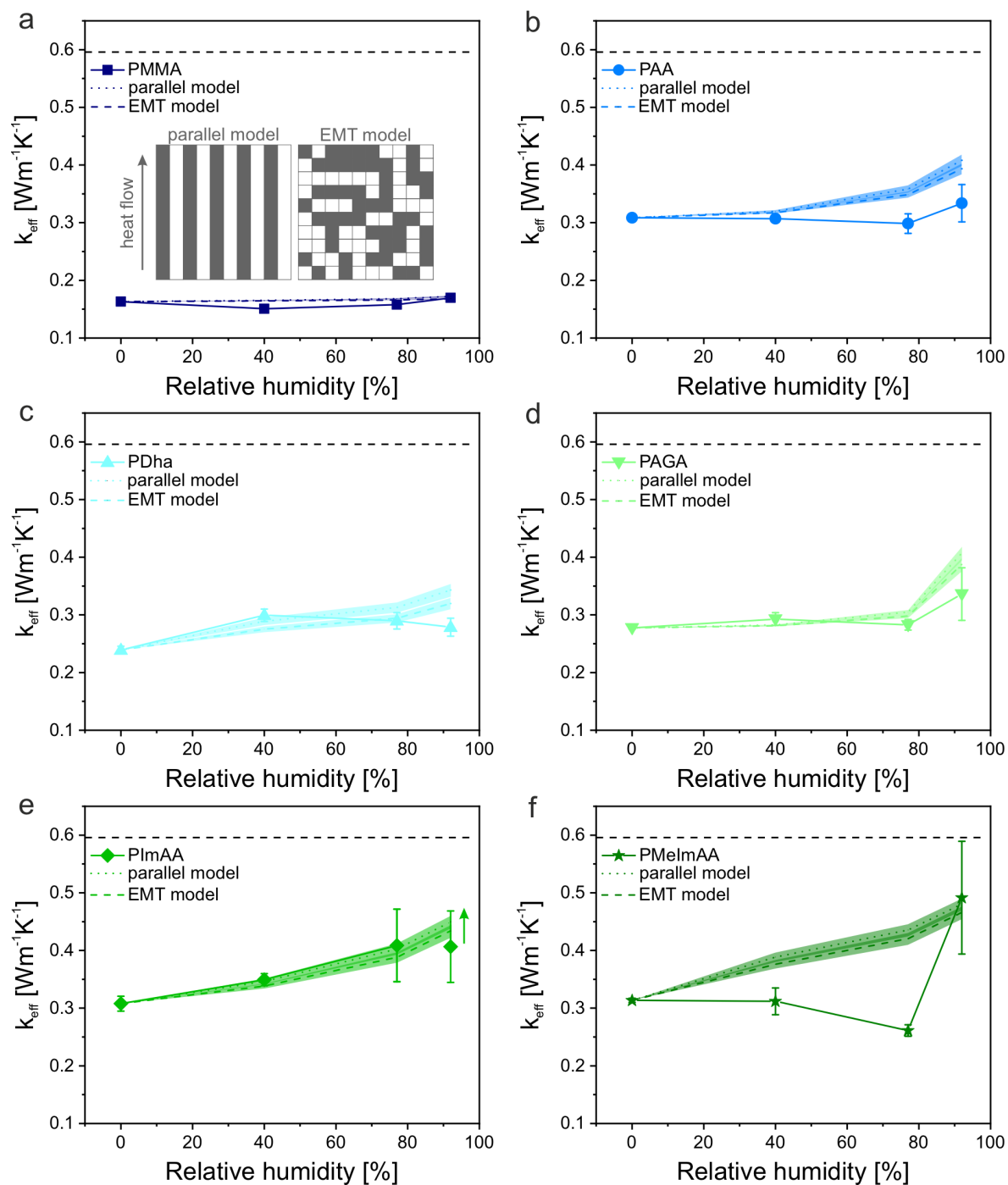


Figure 5. Effective thermal conductivity versus relative humidity for all investigated polymer samples. From (a) to (f) PMMA, PAA, PDha, PAGA, PIImAA, and PMelMAA. The solid symbols

depict the experimental data, while the dashed and dotted lines are calculated values using the parallel and the EMT mixing model, respectively. A schematic illustration of these models is shown as an inset in (a). The shaded areas consider the variability due to the deviation of the moisture content determination. The dashed black line represents the thermal conductivity of water.

The parallel mixing model is based on the presence of extended percolation paths through the entire polymer structure. In contrast, if the water uptake happened in a random and dispersed fashion within the polymer, it should be better represented by the EMT mixing model (also compare to the schematic depiction in the inset of Figure 5a)⁴¹. The small difference between the pure polymer and the pure water thermal conductivity prevents an unambiguous judgment on the presence of dispersed or percolated water inside the polymer. Both mixing models, however, support the straight-forward interpretation in the sense of a water-polymer nanocomposite material. Only the ionic PMeImAA sample deviates strongly from the mixing models, which could be understood in a way that the uptake of water first disrupts thermal transport pathways. Once water condensation sets in at very high humidity (RH ~ 92 %), the thermal conductivity is again dominated by the water-phase.

Conclusion

We employed a set of polyampholytes featuring a high density of functional groups to investigate how thermal transport can be controlled by hydrogen bonding in amorphous polymers. We, therefore, compared four types of ampholytic polymers to PAA and PMMA as reference materials. The investigation of ampholytic polymers is particularly interesting since this opens an elegant pathway to study the influence of H-donor and H-acceptor groups in a one-phase system.

We employed a detailed IR spectroscopy investigation for a holistic understanding of the involved H-bond motifs.

In summary, we can deduce three major trends. Firstly, PAA is an exceptionally well-conducting hydrophilic polymer, which we attribute to a stretched polymer conformation. Secondly, for all ampholytic polymers, we find an overall trend of increasing thermal conductivity along with an increase in the H-bond strength under dry conditions. This can be deduced from a systematic red-shift of the carbonyl peak. Thirdly, the presence of humidity leads to a polymer-specific uptake of water and, consequently, to a variety of changes to the H-bond motifs. Yet, the thermal transport in ampholytic polymers can be well described by mixing models, where the uptake of water is considered as the formation of a nanocomposite material. Deviations from this straight-forward description are PAA, where a high amount of strongly bound water is observed, and for PMeImAA, where ionic interactions are dominant. The deconvolution of the carbonyl resonance peak demonstrates a range of binding motifs between the respective polymers. However, an unambiguous assignment of a particular H-bond moiety to an increased or decreased thermal transport behavior is not possible. Additional factors such as scattering effects along the polymer backbone or on polymer side groups have to be taken into account, as well as subtle changes to the polymer conformation. Overall, our contribution adds to a better understanding of the role of H-bonds for thermal transport in polymer materials.

Most importantly, not only the specific design of H-bond motifs determines the capability to conduct thermal energy. Even in the case of one-phase systems, the various influences of polymer conformation, side-groups, and interaction have to be balanced. We are still far away from a predictive model to molecularly design amorphous polymers to a specific high or low thermal

conductivity. This is an ongoing challenge to be addressed by polymer chemists and engineers over the next years.

ASSOCIATED CONTENT

Supporting Information

thermal conductivity measurements, IR spectroscopy of individual polymers, DSC measurements, effective medium mixing models, and microscopy of the transducer layer

Corresponding Author

*Markus Retsch - Department of Chemistry, Physical Chemistry I, University of Bayreuth, Universitätsstraße 30, 95447 Bayreuth, Germany, ORCID: orcid.org/0000-0003-2629-8450, Email: markus.retsch@uni-bayreuth.de

Author Contributions

The manuscript was written through the contributions of all authors. All authors have given approval to the final version of the manuscript.

Funding Sources

Volkswagen Foundation (Lichtenberg professorship); SFB 840 (project B7); DFG RE3550/2-1; VISIRday ERC StG #714968; SCHA1640/12-1; SFB 1278 “PolyTarget” (project number 316213987, project C03); Carl-Zeiss-Foundation (fellowship for L. W.);

Notes

The authors declare no competing financial interests.

ACKNOWLEDGEMENT

This project was funded through a Lichtenberg professorship by the Volkswagen Foundation and by the German Research Foundation by the SFB 840 (project B7). Additional support was provided by ERC StG VISIRday #714968, DFG RE3550/2-1, SCHA1640/12-1, and the collaborative research center SFB 1278 “PolyTarget” (project number 316213987, project C03). P. B. (Landesgraduiertenstipendium) and L. W. (Carl-Zeiss-Foundation) are grateful for Ph.D. fellowships.

REFERENCES

(1) Moore, A. L.; Shi, L. Emerging challenges and materials for thermal management of electronics. *Mater. Today* **2014**, *17* (4), 163-174, DOI: <https://doi.org/10.1016/j.mattod.2014.04.003>.

(2) Wang, X. J.; Ho, V.; Segalman, R. A.; Cahill, D. G. Thermal Conductivity of High-Modulus Polymer Fibers. *Macromolecules* **2013**, *46* (12), 4937-4943, DOI: 10.1021/ma400612y.

(3) Shen, S.; Henry, A.; Tong, J.; Zheng, R.; Chen, G. Polyethylene nanofibres with very high thermal conductivities. *Nature Nanotechnology* **2010**, *5* (4), 251-255, DOI: 10.1038/nnano.2010.27.

(4) Zhong, Z.; Wingert, M. C.; Strzalka, J.; Wang, H.-H.; Sun, T.; Wang, J.; Chen, R.; Jiang, Z. Structure-induced enhancement of thermal conductivities in electrospun polymer nanofibers. *Nanoscale* **2014**, *6* (14), 8283-8291, DOI: 10.1039/C4NR00547C.

(5) Singh, V.; Bougher, T. L.; Weathers, A.; Cai, Y.; Bi, K.; Pettes, M. T.; McMenamin, S. A.; Lv, W.; Resler, D. P.; Gattuso, T. R.; Altman, D. H.; Sandhage, K. H.; Shi, L.; Henry, A.; Cola,

B. A. High thermal conductivity of chain-oriented amorphous polythiophene. *Nat Nanotechnol* **2014**, *9* (5), 384-90, DOI: 10.1038/nnano.2014.44.

(6) Henry, A.; Chen, G. High Thermal Conductivity of Single Polyethylene Chains Using Molecular Dynamics Simulations. *Phys. Rev. Lett.* **2008**, *101* (23), 235502, DOI: 10.1103/PhysRevLett.101.235502.

(7) Liu, J.; Yang, R. Length-dependent thermal conductivity of single extended polymer chains. *Phys. Rev. B* **2012**, *86* (10), 104307, DOI: 10.1103/PhysRevB.86.104307.

(8) Zhang, T.; Luo, T. Role of Chain Morphology and Stiffness in Thermal Conductivity of Amorphous Polymers. *The Journal of Physical Chemistry B* **2016**, *120* (4), 803-812, DOI: 10.1021/acs.jpcc.5b09955.

(9) Lu, Y.; Liu, J.; Xie, X.; Cahill, D. G. Thermal Conductivity in the Radial Direction of Deformed Polymer Fibers. *Acs Macro Letters* **2016**, *5* (6), 646-650, DOI: 10.1021/acsmacrolett.6b00048.

(10) Huang, C.; Qian, X.; Yang, R. Thermal conductivity of polymers and polymer nanocomposites. *Materials Science and Engineering: R: Reports* **2018**, *132*, 1-22, DOI: <https://doi.org/10.1016/j.mser.2018.06.002>.

(11) Kim, H. S.; Jang, J.-u.; Lee, H.; Kim, S. Y.; Kim, S. H.; Kim, J.; Jung, Y. C.; Yang, B. J. Thermal Management in Polymer Composites: A Review of Physical and Structural Parameters. *Adv. Eng. Mater.* **2018**, *20* (10), 1800204, DOI: 10.1002/adem.201800204.

(12) Song, N.; Jiao, D.; Cui, S.; Hou, X.; Ding, P.; Shi, L. Highly Anisotropic Thermal Conductivity of Layer-by-Layer Assembled Nanofibrillated Cellulose/Graphene Nanosheets

Hybrid Films for Thermal Management. *ACS Appl Mater Interfaces* **2017**, *9* (3), 2924-2932, DOI: 10.1021/acsami.6b11979.

(13) Wang, Z.; Rolle, K.; Schilling, T.; Hummel, P.; Philipp, A.; Kopera, B. A. F.; Lechner, A. M.; Retsch, M.; Breu, J.; Fytas, G. Tunable Thermoelastic Anisotropy in Hybrid Bragg Stacks with Extreme Polymer Confinement. *Angew. Chem. Int. Ed. Engl.* **2020**, *59* (3), 1286-1294, DOI: 10.1002/anie.201911546.

(14) Xie, X.; Li, D. Y.; Tsai, T. H.; Liu, J.; Braun, P. V.; Cahill, D. G. Thermal Conductivity, Heat Capacity, and Elastic Constants of Water Soluble Polymers and Polymer Blends. *Macromolecules* **2016**, *49* (3), 972-978, DOI: 10.1021/acs.macromol.5b02477.

(15) Xie, X.; Yang, K.; Li, D.; Tsai, T.-H.; Shin, J.; Braun, P. V.; Cahill, D. G. High and low thermal conductivity of amorphous macromolecules. *Phys. Rev. B* **2017**, *95* (3), 035406.

(16) Shanker, A.; Li, C.; Kim, G. H.; Gidley, D.; Pipe, K. P.; Kim, J. High thermal conductivity in electrostatically engineered amorphous polymers. *Sci Adv* **2017**, *3* (7), e1700342, DOI: 10.1126/sciadv.1700342.

(17) Kim, G. H.; Lee, D.; Shanker, A.; Shao, L.; Kwon, M. S.; Gidley, D.; Kim, J.; Pipe, K. P. High thermal conductivity in amorphous polymer blends by engineered interchain interactions. *Nat Mater* **2015**, *14* (3), 295-300, DOI: 10.1038/nmat4141.

(18) Rössel, C.; Billing, M.; Görls, H.; Festag, G.; Grube, M.; Bellstedt, P.; Nischang, I.; Schacher, F. H. Synthesis and modification of poly(ethyl 2-(imidazol-1-yl)acrylate) (PEImA). *Polymer* **2017**, *127*, 182-191, DOI: <https://doi.org/10.1016/j.polymer.2017.08.058>.

(19) Günther, U.; Sigolaeva, L. V.; Pergushov, D. V.; Schacher, F. H. Polyelectrolytes with Tunable Charge Based on Polydehydroalanine: Synthesis and Solution Properties. *Macromol. Chem. Phys.* **2013**, *214* (19), 2202-2212, DOI: 10.1002/macp.201300324.

(20) von der Lühe, M.; Weidner, A.; Dutz, S.; Schacher, F. H. Reversible Electrostatic Adsorption of Polyelectrolytes and Bovine Serum Albumin onto Polyzwitterion-Coated Magnetic Multicore Nanoparticles: Implications for Sensing and Drug Delivery. *ACS Applied Nano Materials* **2018**, *1* (1), 232-244, DOI: 10.1021/acsnm.7b00118.

(21) Sidot, C.; Christidis, Y. Amides α,β -éthyléniques N-alcoylolées et leur procédé de fabrication. EP0284481 B1, June 9, 1964.

(22) Volkmann, L.; Köhler, M.; Sobotta, F. H.; Enke, M. T.; Brendel, J. C.; Schacher, F. H. Poly(2-acrylamidoglycolic acid) (PAGA): Controlled Polymerization Using RAFT and Chelation of Metal Cations. *Macromolecules* **2018**, *51* (18), 7284-7294, DOI: 10.1021/acs.macromol.8b01260.

(23) Mayadunne, R. T. A.; Rizzardo, E.; Chiefari, J.; Krstina, J.; Moad, G.; Postma, A.; Thang, S. H. Living Polymers by the Use of Trithiocarbonates as Reversible Addition–Fragmentation Chain Transfer (RAFT) Agents: ABA Triblock Copolymers by Radical Polymerization in Two Steps. *Macromolecules* **2000**, *33* (2), 243-245, DOI: 10.1021/ma991451a.

(24) Winston, P. W.; Bates, D. H. Saturated Solutions For the Control of Humidity in Biological Research. *Ecology* **1960**, *41* (1), 232-237, DOI: 10.2307/1931961.

(25) Hu, H. P.; Wang, X. W.; Xu, X. F. Generalized theory of the photoacoustic effect in a multilayer material. *J. Appl. Phys.* **1999**, *86* (7), 3953-3958, DOI: Doi 10.1063/1.371313.

- (26) Wang, X.; Hu, H.; Xu, X. Photo-Acoustic Measurement of Thermal Conductivity of Thin Films and Bulk Materials. *J. Heat Transfer* **2001**, *123* (1), 138-144, DOI: 10.1115/1.1337652.
- (27) Park, Y.; Lee, S.; Ha, S. S.; Alunda, B.; Noh, D. Y.; Lee, Y. J.; Kim, S.; Seol, J. H. Crosslinking Effect on Thermal Conductivity of Electrospun Poly(acrylic acid) Nanofibers. *Polymers* **2019**, *11* (5), 858.
- (28) Kauppinen, J. K.; Moffatt, D. J.; Mantsch, H. H.; Cameron, D. G. Fourier Self-Deconvolution: A Method for Resolving Intrinsically Overlapped Bands. *Appl. Spectrosc.* **1981**, *35* (3), 271-276.
- (29) Hu, X.; Kaplan, D.; Cebe, P. Determining Beta-Sheet Crystallinity in Fibrous Proteins by Thermal Analysis and Infrared Spectroscopy. *Macromolecules* **2006**, *39* (18), 6161-6170, DOI: 10.1021/ma0610109.
- (30) Thomas, L. C. Modulated DSC Basics; Optimization of MDSC Experimental Conditions *Modulated DSC Paper* [Online], 2005. http://www.tainstruments.com/pdf/literature/TP_008_MDSC_num_3_Optimization_of_Experimental_Conditions.pdf (accessed 08.11.2019).
- (31) Dong, J.; Ozaki, Y.; Nakashima, K. Infrared, Raman, and Near-Infrared Spectroscopic Evidence for the Coexistence of Various Hydrogen-Bond Forms in Poly(acrylic acid). *Macromolecules* **1997**, *30* (4), 1111-1117, DOI: 10.1021/ma960693x.
- (32) Coleman, M. M.; Sobkowiak, M.; Pehlert, G. J.; Painter, P. C.; Iqbal, T. Infrared temperature studies of a simple polyurea. *Macromol. Chem. Phys.* **1997**, *198* (1), 117-136, DOI: 10.1002/macp.1997.021980110.

(33) Skrovanek, D. J.; Howe, S. E.; Painter, P. C.; Coleman, M. M. Hydrogen bonding in polymers: infrared temperature studies of an amorphous polyamide. *Macromolecules* **1985**, *18* (9), 1676-1683, DOI: 10.1021/ma00151a006.

(34) Skrovanek, D. J.; Painter, P. C.; Coleman, M. M. Hydrogen bonding in polymers. 2. Infrared temperature studies of nylon 11. *Macromolecules* **1986**, *19* (3), 699-705, DOI: 10.1021/ma00157a037.

(35) Shen, Z.; Luo, F.; Bai, H.; Si, P.; Lei, X.; Ding, S.; Ji, L. A study on mediating the crystallization behavior of PBT through intermolecular hydrogen-bonding. *RSC Advances* **2016**, *6* (21), 17510-17518, DOI: 10.1039/C5RA25438H.

(36) Daniliuc, L.; David, C. Intermolecular interactions in blends of poly(vinyl alcohol) with poly(acrylic acid): 2. Correlation between the states of sorbed water and the interactions in homopolymers and their blends. *Polymer* **1996**, *37* (23), 5219-5227, DOI: [https://doi.org/10.1016/0032-3861\(96\)00328-X](https://doi.org/10.1016/0032-3861(96)00328-X).

(37) Wieland, M.; Dingler, C.; Merkle, R.; Maier, J.; Ludwigs, S. Humidity-Controlled Water Uptake and Conductivities in Ion and Electron Mixed Conducting Polythiophene Films. *ACS Appl Mater Interfaces* **2020**, *12* (5), 6742-6751, DOI: 10.1021/acsami.9b21181.

(38) Popineau, S.; Rondeau-Mouro, C.; Sulpice-Gaillet, C.; Shanahan, M. E. R. Free/bound water absorption in an epoxy adhesive. *Polymer* **2005**, *46* (24), 10733-10740, DOI: <https://doi.org/10.1016/j.polymer.2005.09.008>.

(39) Ichikawa, K.; Mori, T.; Kitano, H.; Fukuda, M.; Mochizuki, A.; Tanaka, M. Fourier transform infrared study on the sorption of water to various kinds of polymer thin films. *J. Polym. Sci., Part B: Polym. Phys.* **2001**, *39* (18), 2175-2182, DOI: 10.1002/polb.1191.

(40) Mehra, N.; Mu, L.; Ji, T.; Li, Y.; Zhu, J. Moisture driven thermal conduction in polymer and polymer blends. *Compos. Sci. Technol.* **2017**, *151*, 115-123, DOI: 10.1016/j.compscitech.2017.08.010.

(41) Carson, J. K.; Lovatt, S. J.; Tanner, D. J.; Cleland, A. C. Thermal conductivity bounds for isotropic, porous materials. *Int. J. Heat Mass Transfer* **2005**, *48* (11), 2150-2158, DOI: 10.1016/j.ijheatmasstransfer.2004.12.032.